Chemical Physics Letters 714 (2019) 94–98

Contents lists available at ScienceDirect

Chemical Physics Letters

journal homepage: www.elsevier.com/locate/cplett

Research paper

Atomistic and coarse-grained modeling of polyethyleneimine

Titus A. Beu*, Andrada E. Ailenei, Alexandra Farcaș

Department of Biomolecular Physics, Faculty of Physics, University Babeș-Bolyai, 1 Mihail Kogălniceanu, Cluj-Napoca 400084, Romania

HIGHLIGHTS

- Residue-based coarse-grained (CG) model for polyethyleneimine (PEI) derived from atomistic (AA) symmetric residue types.
- Reduced number of bead types which coincide with entire symmetric residues.
- Simple definition of chains of arbitrary size and protonation pattern.
- Very good agreement of the CG results both with the AA simulations and the experimental evidence.
- Applicability of the CG FF in realistic large-scale simulations of DNA-PEI condensation.

ARTICLE INFO

Keywords:
Cationic polymers
Polyethyleneimine
Force fields
Molecular dynamics
Coarse-graining

ABSTRACT

As a widely used non-viral gene delivery vector, polyethyleneimine (PEI) was investigated at all-atom (AA) and coarse-grained (CG) levels. We used our recently published AA (CHARMM) force-field for PEI in extensive molecular dynamics (MD) simulations, from which we extracted probability distributions for the distances, angles, and dihedrals formed by the residues. These were further employed to parametrize a CG (MARTINI) force field, which was fine-tuned by fitting the simulated CG structural and dynamical properties to their AA counterparts. The developed AA and CG force fields are suitable for realistic large-scale simulations of PEI-DNA condensation.

1. Introduction

Polyethyleneimine, $-[CH_2–NH–CH_2]_n–$, is one of the most widely used non-viral gene delivery vectors. Its transfection efficiency is linked to the high buffering capacity that can be achieved by particular patterns of protonated amino groups. It is presently accepted that the condensation of DNA and formation of polyplexes thereof apt to enter cells via endocytosis are conditioned to a large extent by the electrostatic interactions between the positive amino groups of PEI and the negative phosphate groups of DNA [1].

The present investigations address two distinct modeling levels of linear PEI chains: all-atom (AA) and coarse-grained (CG). Specifically, we employed an all-atom CHARMM [2] force field for PEI [3] (a revised version of a previous model [4]), based on symmetric residues and with the FF parameters optimized relative to high-quality ab initio calculations on a set of model polymers. Unlike other AA FFs for PEI reported in the literature [5–7], we consistently optimized not only the dihedral parameters, but also the bond and angle parameters, along with the partial atomic charges. We carried out comprehensive MD simulations and published a detailed analysis of the structural and dynamical behavior for PEI chains of various lengths and protonation patterns (such as gyration radius, end-to-end distance, diffusion coefficient). From AA trajectories we constructed as part of the present work probability distributions for the distances, angles, and dihedrals formed by the residues, which we used to parametrize a MARTINI force field [8] for CG beads (identified with entire residues). The Boltzmann inversion methodology [9] used to generate the CG bonded parameters was complemented with an additional model to combine the regression parameters resulted for the *multi-peak* probability distributions. We performed CG simulations for PEI chains of sizes and protonation patterns similar to the atomistic ones and, finally, fine-tuned the CG FF by matching the obtained CG structural and dynamical properties with their AA counterparts. The quality of the CG FF is validated by the fair agreement between the simulated diffusion coefficients and the experimental evidence. In conjunction with existing CHARMM and MARTINI FFs for DNA, the elaborated AA and CG FFs for PEI are suitable for realistic large-scale simulations of solvated PEI-DNA polyplexes.

* Corresponding author.
E-mail address: titus.beu@phys.ubbcluj.ro (T.A. Beu).

https://doi.org/10.1016/j.cplett.2018.10.071
Received 21 September 2018; Received in revised form 18 October 2018; Accepted 30 October 2018
Available online 31 October 2018

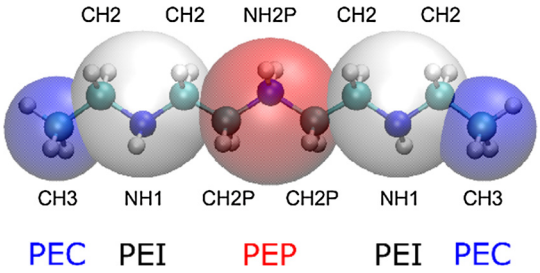

Fig. 1. Backbone atom types (NH1, CH2, NH2P, CH2P, and CH3) and residue types (PEI, PEP, and PEC) on which our atomistic force-field model relies. Within the coarse-grained force-field model, the beads are identified with entire residues.

2. Methods

Our CHARMM FF relies on three residue types reflecting the main chemical groups present in the modeled PEI chains:

- PEI – generic unprotonated monomer –[CH_2–NH–CH_2]–,
- PEP – protonated monomer –[CH_2–NH_2^+–CH_2]–, and
- PEC – CH_3 group starting/ending the PEI chains.

We accounted for the representative vicinities of the backbone atoms (see Fig. 1) by defining nine atom types: NH1 and HNH1 for the N and H atoms of the NH-group within the PEI residue; NH2P and HN2P for the protonated NH_2^+-group within the PEP residue; CH2 and HC2 for the CH_2-group within the PEI residue; CH2P for the C of the CH_2-group within the PEP residue; CH3 and HC3 for the terminal CH3-group (PEC residue).

As applicable to the specific PEI polymers studied, from among the bonded terms defined by the standard CHARMM FF, we considered only those modeling valence bonds, bond angles, and dihedral angles:

$$U_{\text{bonded}} = \sum_{\text{bonds}} k_b (b - b_0)^2 + \sum_{\text{angles}} k_\theta (\theta - \theta_0)^2 + \sum_{\text{dihedrals}} k_\psi [1 + \cos(n\psi - \delta)],$$

where k_b, k_θ, and k_ψ are force constants, b_0 and θ_0 are equilibrium bonds and angles, while n and δ are dihedral multiplicities and shifts. The non-bonded interactions were modeled by Coulomb and Lennard-Jones (LJ) terms:

$$U_{\text{non-bonded}} = \sum_{\text{atoms } i,j} \left\{ \frac{q_i q_j}{\varepsilon_0 r_{ij}} + \varepsilon_{ij} \left[\left(\frac{r_{ij}^{\min}}{r_{ij}} \right)^{12} - 2 \left(\frac{r_{ij}^{\min}}{r_{ij}} \right)^{6} \right] \right\},$$

with q_i atomic charges, r_{ij} interatomic distances, $r_{ij}^{\min} = (r_i^{\min} + r_j^{\min})/2$ and $\varepsilon_{ij} = \sqrt{\varepsilon_i \varepsilon_j}$ Lennard-Jones radii and potential well depths, respectively.

For parametrizing our atomistic CHARMM FF we defined three PEI model pentamers: one unprotonated, one singly-protonated at the central monomer, and one alternatively (doubly) protonated. For each of them we performed quantum mechanical (QM) calculations at MP2/6-31G(d) level for equilibrium and distorted configurations, which we used to adjust the parameters of the CHARMM FF by following the methodology implemented in the Force-Field Tool Kit (ffTK) [10]. We consistently optimized the whole set of bonded parameters, along with the atomic charges, essentially, by carrying out the following steps:

1. Assigning Lennard-Jones parameters to each atom type by analogy with standard CHARMM types.
2. Adjusting the partial atomic charges with respect to QM PEI-water interaction profiles and dipole moments.
3. Optimizing the bond- and angle parameters by matching QM and molecular mechanics (MM) distortion energies determined from Hessian matrices in internal coordinates.
4. Adjusting the dihedral parameters using explicit QM scans of the dihedrals, by matching the QM and MM torsion energy surfaces.

The CG MARTINI FF comprises similar terms referring to *beads*. Nevertheless, instead of the cosine-dependent bond-angle contributions, $1/2 \sum k_\theta (\cos\theta - \cos\theta_0)^2$, as in the original definition of MARTINI [8], which occasionally lead to instabilities, based on a careful analysis of the probability distributions, we chose simple angle-dependent potential energy terms, $1/2 \sum k_\theta (\theta - \theta_0)^2$, as in the CHARMM FF. The standard MARTINI approach does not include dihedral terms, but torsion is required here as a fine-tuning component of the CG potential model. The beads can be seen in Fig. 1 to coincide with the centers of mass of entire residues and bear the same names: PEI–generic unprotonated monomer (white), PEP–protonated monomer (red), and PEC–terminal methyl group (blue).

All MD simulations were carried out with the NAMD code [11] using a radial cutoff of 12 Å and a switching distance of 10 Å for the short-range interactions, and applying periodic boundary conditions in all three directions. The electrostatics was treated in the AA case by the Particle Mesh Ewald approach using a 1 Å grid spacing, while in the CG case we employed (as per current practice) an increased relative dielectric constant set to 15. A Langevin thermostat was used to fix the temperature at 310 K and the pressure was set to 1 atm using a Langevin piston. We used a time step of 2 fs in the AA simulations and 10 fs in the CG simulations.

3. Results and discussion

To investigate the structural and dynamical behavior of PEI in dependence on the length and protonation pattern, we carried out MD simulations on chains composed of $12n + 3$ monomers (27-mer, 39-mer, and 51-mer), unprotonated or uniformly protonated in ratios equal to 1/4 (one-in-four), 1/3 (one-in-three), and 1/2 (alternative protonation). A snapshot from a typical atomistic trajectory is depicted in Fig. 2a.

With a view to achieving superior statistics, for each of the three considered polymer lengths and four protonation patterns, instead of considering a single trajectory, we actually cumulated a total of 400 ns of data collection from 20 successive runs. Each trajectory extended over 21 ns and adopted the initial configuration from the last frame of the previous one, however, with the first nanosecond discarded to reduce time correlations.

In our previous paper [3], we characterized the dynamic structuring of the solvated PEI chains by means of gyration radius and end-to-end distance. For instance, the time- and ensemble-averaged gyration radius for the unprotonated and the 1/2-protonated 51-mers were respectively found equal to 15.8 and 29.1 Å, showing a somewhat increased rigidity compared to the values reported by Choudhury et. al. [6] for 50-mers, i.e. 12.3 and 24.1 Å, respectively. Interestingly, the unprotonated PEI chains was found to also comply with the continuous worm-like chain model [12] (featuring a persistence length of about 4 Å), which, however, does not apply in the case of protonated PEI chains, essentially owing to the non-identical beads and the supplementary electrostatic interactions. The diffusion coefficient that we obtained [3] for the unprotonated PEI 51-mer, i.e. 1.2×10^{-6} cm^2/s, practically coincides with the experimental result of Clamme et al. [13].

From the AA trajectories, we constructed targeted probability distributions to serve the subsequent derivation of the CG FF. Fig. 3 shows for illustration the calculated time- and ensemble-averaged probability distribution for the distance between the centers of mass of adjacent PEC-PEI residues, along with a three-peak fit and an average single-peak function. Similar multi-function distributions were also obtained for the bond angles and dihedral angles formed by the residues.

As compared to AA simulations, coarse-graining typically enables both significantly reducing the number of simulated particles (roughly

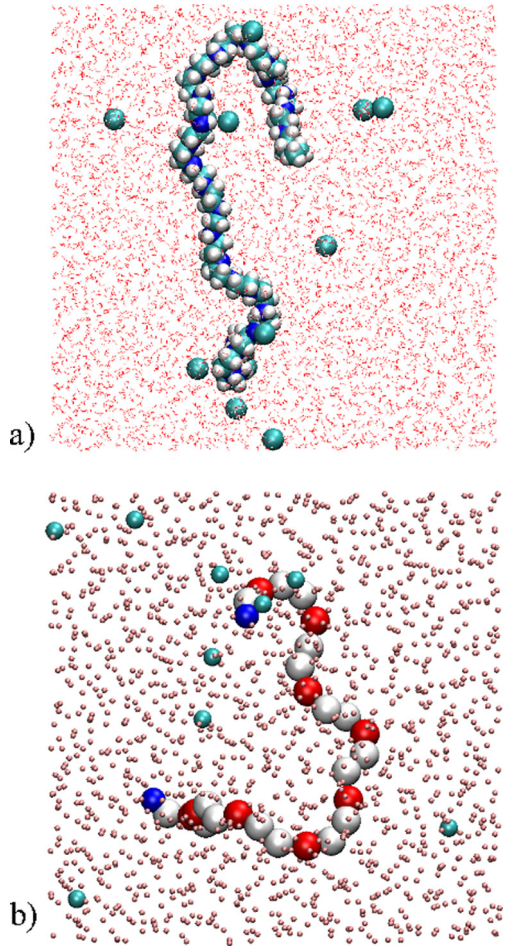

Fig. 2. Snaphots from typical (a) atomistic and (b) coarse-grained trajectories of the 1/3-protonated PEI 27-mer.

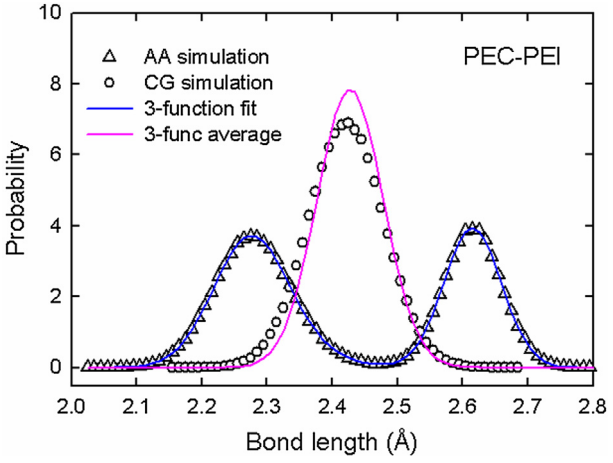

Fig. 3. Comparison of the AA and CG PEC-PEI distance distributions. With continuous lines, three-peak fit of the AA distribution (blue) and average single-peak model (pink) used to derive the CG parameters.(For interpretation of the references to colour in this figure legend, the reader is referred to the web version of this article.)

by an order of magnitude) and increasing the time step. Altogether, both aspects lead to a significant reduction of the CPU time per step, allowing for qualitatively superior space- and time scales to be achieved.

The MARTINI FF employs a four-to-one mapping, i.e. four heavy atoms are represented on average by a single CG bead. Four main types of interaction sites are being considered (P–polar, N–nonpolar, C–apolar, and Q-charged), with four subtypes (d–donor, a–acceptor, da–both, and 0–none) and 10 interaction levels. The water beads, modeled by definition as P4 sites, represent four water molecules and are replaced in a 1-to-10 ratio by antifreeze particles BP4 to prevent artificial freezing. As can be seen in Fig. 1, the three specific CG bead types that we defined (PEC, PEI, and PEP) respectively comprise one, three, and three heavy atoms, and were respectively modeled as SN0, SN0, and SQ0 sites. The additional "S" designates smaller bead variants, which are packed more closely together, more precisely, with the LJ potential minimum reduced by 0.4 Å and the well depth by 25%. According to common practice, the Cl^- counterions added to neutralize the protonated PEI chains were modeled as Qa beads. In the CG simulations, the masses of the PEC, PEI, and PEP beads were set equal to the respective sums of atomic masses.

In parametrizing the MARTINI FF for PEI, we considered neutral PEC and PEI beads, attributed unitary charge to the PEP bead, and identified the non-bonded LJ parameters with those of the associated standard MARTINI bead types (SN0, SN0, and SQ0). We actually tested thoroughly a whole series of combinations of neutral and charged MARTINI bead types and obtained the closest agreement with the size and protonation dependences of the AA gyration radius, end-to-end distance, and diffusion coefficient by using the mentioned "small" types. To determine the bonded parameters, we applied the Boltzmann inversion technique [9] to AA probability distributions for distances, angles, and dihedral angles formed by the centers of mass of adjacent residues (beads). These distributions were actually obtained by averaging over the entire ensemble of AA trajectories, irrespective of chain size and protonation pattern. As illustrated by Fig. 3 for the PEC-PEI distance probability, these distributions feature by no means a single peak, as might be desirable for a straightforward application of the Boltzmann inversion.

To match their typical multi-peak structure, reflecting stretches and rotations with different tacticity along the chain, for the probability distributions of the distances b and angles θ between two and, respectively, three adjacent residues, we considered three-peak fit functions:

$$P = \sum_{i=1}^{3} A_i e^{-U_i/k_B T},$$

with harmonic potential energy contributions:

$$U_i^b = \frac{1}{2} k_{b,i}(b - b_{0,i})^2, \quad U_i^\theta = \frac{1}{2} k_{\theta,i}(\theta - \theta_{0,i})^2.$$

Since, for a given combination of residues, the NAMD code does not operate with multiple bond and angle parameters, we defined the final CG force constants, equilibrium bond lengths, and equilibrium angles as weighted averages of the individual-peak values, using as weights the peak areas.

Fig. 3 comparatively shows the time- and ensemble-averaged AA and CG probability distributions for the PEC-PEI distance. Similarly, the AA and CG probability distributions for the PEC-PEI-PEP angle are plotted in Fig. 4. We note the fair agreement between the simulated CG probability distributions and the 3-peak-average models applied to extract the parameters used in the CG simulations.

Given the qualitatively different probability distributions for dihedral angles between the centers of mass of four adjacent residues (see Fig. 5), we used in this case a four-function fit:

$$P_\psi = A e^{-U_\psi/k_B T}$$

where

$$U_\psi = \sum_{i=1}^{4} K_{\psi,i}[1 + \cos(n_i \psi - \delta_i)]$$

with multiplicities $n_i = 1, 2, 3, 4$ and shifts $\delta_i = 0$ or 180°.

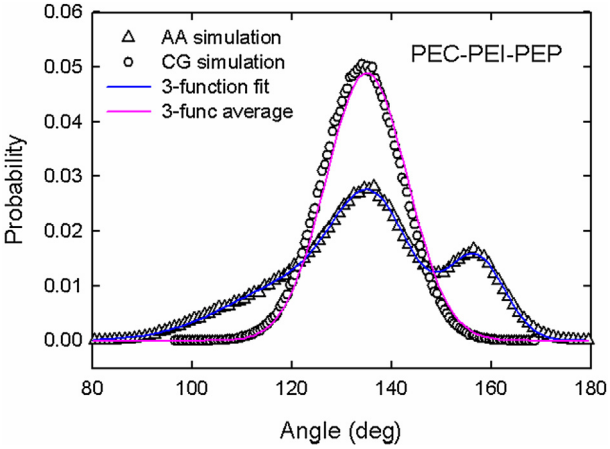

Fig. 4. Comparison of the AA and CG PEC-PEI-PEP angle distributions, along with the three-peak fit of the AA distribution (blue) and average single-peak model (pink) used to derive the CG parameters.(For interpretation of the references to colour in this figure legend, the reader is referred to the web version of this article.)

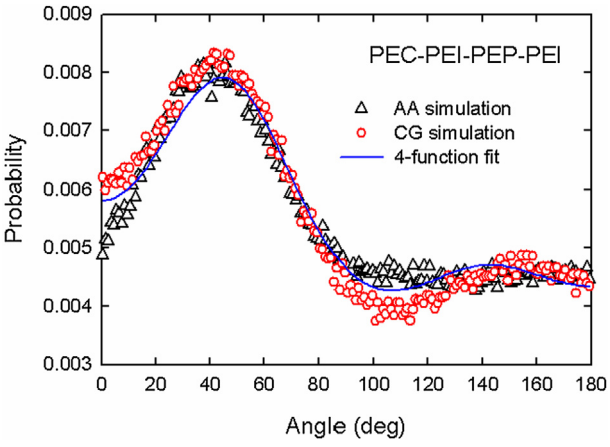

Fig. 5. Comparison of the AA and CG PEC-PEI-PEP-PEI dihedral-angle distributions. With continuous blue line, four-function fit of the AA distribution.

Fig. 5 shows for dihedral angles that the CG profile is consistent both with the AA distribution and the multi-function fit model. The slight deviations between the AA and CG distributions can be ascribed to the presence of the protonated residues (PEP) and the fact that NAMD implements different AA and CG approaches for the electrostatics, as mentioned in the Methods section. Also, the better agreement of the AA and CG distributions for bonds, angles, and dihedrals involving exclusively PEI residues as compared to those also including PEP residues is clearly determined by the larger occurrence frequency of PEI residues in the entire set of polymers (for all protonation fractions) used in the averaging procedure.

A typical snapshot of a CG trajectory for the solvated 1/3-protonated PEI 27-mer is illustrated in Fig. 2b. Fig. 6 depicts the time dependences of the gyration radius (R_g) for the whole ensemble of 50 trajectories generated for the 1/3-protonated PEI 51-mer. In spite of the huge instantaneous fluctuations, the ensemble-averaged time dependence of R_g (plotted with black) is rather smooth. As global indication of the polymer size, the ensemble- and time-averaged gyration radius can be seen in Fig. 7 to depend quasi-linearly on the chain length. As expected, unprotonated chains are the most compact, while, due to the additional Coulomb repulsion, increasing protonation (1/3, for illustration) brings about more expanded spatial configurations. The low error bars are a positive result of the combined ensemble- and time averaging procedure applied to the large sets of simulated trajectories.

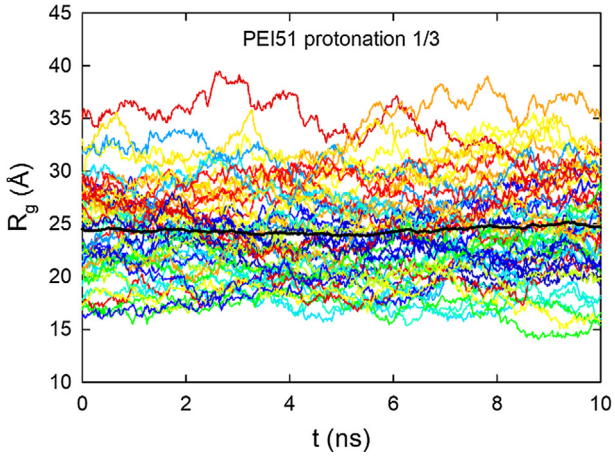

Fig. 6. Time evolution of the gyration radius for an ensemble of 50 CG trajectories run for the 1/3-protonated PEI 51-mer, along with the ensamble-averaged dependence (black).

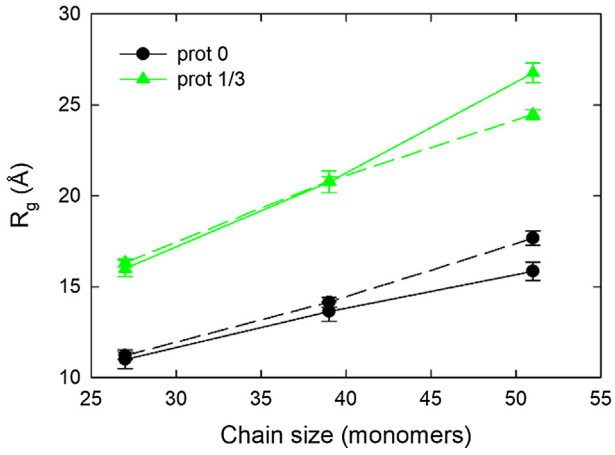

Fig. 7. Size dependence of the ensemble- and time-averaged gyration radius of the AA (solid line) and CG (dashed line) PEI chains for different protonation fractions (unprotonated and 1/3 protonation).

The polymer-length and protonation-fraction dependences of the gyration radius and end-to-end distance show remarkable consistency with the AA results. However, a degradation of the agreement is noted for increasing protonation fraction. In fact, the relative deviation of the CG results from the AA values of the gyration radius reaches 12.5% for the alternatively protonated 51-mer. This appears to be a direct consequence of the different approaches implemented for the electrostatics in AA and CG simulations, as mentioned in the Methods section.

The standard MARTINI water model (90% P4 and 10% BP4 beads) is found to overestimate the attraction between the Cl^- ions and the charged PEP beads. Indeed, the PEP beads, being screened by the large Cl^- (Qa type) beads, appear to experience underestimated mutual repulsion, resulting in reduced gyration radii (see Fig. 7).

Based on the generally accepted interpretation of the time scale in CG simulations, due to the smoother energy landscapes resulting from the larger particle sizes, the scaling of the permeation rates and diffusion coefficients by a factor of about 4 is recommended [8]. Indeed, if scaled by 4, our apparently underestimated CG diffusion coefficient for the unprotonated 51-mer ($0.25 \times 10^{-6}\,cm^2/s$) becomes fairly consistent both with our AA result and the experimental value of Clamme et al. ($1.2 \times 10^{-6}\,cm^2/s$) [13].

4. Conclusion

We present a novel coarse-grained (CG) model for protonated/unprotonated polyethyleneimine (PEI), complying with the MARTINI force field (FF) standard. The non-bonded interactions are treated by assigning the defined CG beads to standard MARTINI types. The bonded contributions to the CG FF are parametrized based on a very large set of all-atom (AA) trajectories for solvated PEI chains of various sizes and protonation patterns, simulated using our recently published atomistic CHARMM FF [3]. The derivation of the CG FF parameters is accomplished by Boltzmann inversion techniques with multi-peak model functions.

The reported MARTINI FF is used to investigate the properties of solvated PEI chains via extensive MD simulations. The very good quality of the FF is confirmed by the close agreement between (a) the CG probability distributions and the modeled AA profiles for bonds, angles, and dihedrals defined by adjacent residues (beads); (b) the AA and CG dynamic structuring (gyration radius and end-to-end distance); and (c) the simulated diffusion coefficients and the experimental evidence.

The present CG PEI model is a promising candidate for massive simulations of PEI-DNA condensation, of utmost importance for developing effective drug-delivery protocols, and qualitatively exceeding the time- and space scales achievable at AA level.

Funding

Work supported by the Executive Unit for Financing Higher Education, Research, Development and Innovation (UEFISCDI), project PN-III-P4-ID-PCE-2016-0474.

References

[1] R. Narain (Ed.), Polymers and Nanomaterials for Gene Therapy, Elsevier; Woodhead Publishing, Cambridge, 2016.
[2] K. Vanommeslaeghe, E. Hatcher, C. Acharya, S. Kundu, S. Zhong, J. Shim, E. Darian, O. Guvench, P. Lopes, I. Vorobyov, A.D. MacKerell Jr, J. Comput. Chem. 31 (2010) 671, https://doi.org/10.1002/jcc.21367.
[3] T.A. Beu, A.E. Ailenei, A. Farcaș, J. Comput. Chem. (2018), https://doi.org/10.1002/jcc.25637 in press.
[4] T.A. Beu, A. Farcaș, J. Comput. Chem. 38 (2017) 2335, https://doi.org/10.1002/jcc.24890.
[5] C. Sun, T. Tang, H. Uludağ, J.E. Cuervo, Biophys. J. 100 (2011) 2754, https://doi.org/10.1016/j.bpj.2011.04.045.
[6] C.K. Choudhury, S. Roy, Soft Matt. 9 (2013) 2269, https://doi.org/10.1039/c2sm26290h.
[7] Z. Wei, E. Luijten, J. Chem. Phys. 143 (2015) 243146, https://doi.org/10.1063/1.4937384.
[8] S.J. Marrink, H.J. Risselada, S. Yefimov, D.P. Tieleman, A.H. de Vries, J. Phys. Chem. B 111 (2007) 7812, https://doi.org/10.1021/jp071097f.
[9] D. Reith, M. Pütz, F. Müller-Plathe, J. Comput. Chem. 24 (2003) 1624, https://doi.org/10.1002/jcc.10307.
[10] C.G. Mayne, J. Saam, K. Schulten, E. Tajkhorshid, J.C. Gumbart, J. Comput. Chem. 34 (2013) 2757, https://doi.org/10.1002/jcc.23422.
[11] J.C. Phillips, R. Braun, W. Wang, J. Gumbart, E. Tajkhorshid, E. Villa, C. Chipot, R.D. Skeel, L. Kale, K. Schulten, J. Comput. Chem. 26 (2005) 1781, https://doi.org/10.1002/jcc.20289.
[12] O. Kratky, G. Porod, Recl. Trav. Chim. Pays. Bas. 68 (1949) 1106, https://doi.org/10.1002/recl.19490681203.
[13] J.P. Clamme, J. Azoulay, Y. Mely, Biophys J. 84 (2003) 1960, https://doi.org/10.1016/S0006-3495(03)75004-8.